Neuronal depletion of calcium-dependent proteins in the dentate gyrus is tightly linked to Alzheimer's disease-related cognitive deficits

Jorge J. Palop*, Brian Jones*, Lisa Kekonius*, Jeannie Chin*, Gui-Qiu Yu*, Jacob Raber*†, Eliezer Masliah‡, and Lennart Mucke*§

*Gladstone Institute of Neurological Disease and Department of Neurology, University of California, San Francisco, CA 94141; and ‡Departments of Neurosciences and Pathology, University of California at San Diego, La Jolla, CA 92093

Communicated by Robert W. Mahley, The J. David Gladstone Institutes, San Francisco, CA, June 3, 2003 (received for review March 20, 2003)

Transgenic mice expressing human amyloid precursor proteins (hAPP) and amyloid-β peptides (Aβ) in neurons develop phenotypic alterations resembling Alzheimer's disease (AD). The mechanisms underlying cognitive deficits in AD and hAPP mice are largely unknown. We have identified two molecular alterations that accurately reflect AD-related cognitive impairments. Learning deficits in mice expressing familial AD-mutant hAPP correlated strongly with decreased levels of the calcium-binding protein calbindin-D_{28k} (CB) and the calcium-dependent immediate early gene product c-Fos in granule cells of the dentate gyrus, a brain region critically involved in learning and memory. These molecular alterations were age-dependent and correlated with the relative abundance of Aβ1–42 but not with the amount of Aβ deposited in amyloid plaques. CB reductions in the dentate gyrus primarily reflected a decrease in neuronal CB levels rather than a loss of CB-producing neurons. CB levels were also markedly reduced in granule cells of humans with AD, even though these neurons are relatively resistant to AD-related cell death. Thus, neuronal populations resisting cell death in AD and hAPP mice can still be drastically altered at the molecular level. The tight link between Aβ-induced cognitive deficits and neuronal depletion of CB and c-Fos suggests an involvement of calcium-dependent pathways in AD-related cognitive decline and could facilitate the preclinical evaluation of novel AD treatments.

The bright prospect of increasing life expectancy in many populations around the world is tempered by an alarming increase in aging-related neurodegenerative disorders (1). Alzheimer's disease (AD), the most frequent of these conditions, causes inexorable loss of memory and other cognitive functions. Although the etiology of most AD cases remains elusive, the analysis of related transgenic (TG) mouse models is beginning to unravel the pathogenic importance of specific AD-associated molecules (2–8). These models are also used increasingly to assess novel AD treatments (9–13). Amyloid plaques are the primary pathological outcome measure in these studies, although their contribution to AD-related cognitive deficits is uncertain (4–6, 8, 14–16). Indeed, there is an urgent need to pinpoint reliable surrogate markers of Aβ-induced cognitive decline and to unravel the pathways that disrupt neuronal functions in AD and related conditions.

We studied TG mice in which neuronal expression of human amyloid precursor proteins (hAPP) is directed by the platelet-derived growth factor β chain promoter (6). Mice from line J20 express familial AD-mutant (K670N, M671L, V717F; hAPP770 numbering) hAPP ($hAPP_{FAD}$) and have high levels of human amyloid-β peptides (Aβ) in the hippocampus (6), which is heavily affected in AD and critically involved in learning and memory (17–19). We analyzed the expression of calcium-dependent proteins in the hippocampus and their relationships with cognitive deficits in $hAPP_{FAD}$ mice and AD, because neuronal calcium homeostasis and calcium signaling likely play critical roles in learning and memory as well as in the pathogenesis of AD (20–23).

Materials and Methods

TG Mice and Behavioral Testing. Line J20 produces hAPP with the Swedish and Indiana FAD mutations; line I5 produces WT hAPP ($hAPP_{WT}$) at comparable levels (6, 24). Mice represent F_6–F_{10} offspring of heterozygous TG mice and C57BL/6J non-TG breeders.

Unless indicated otherwise, measurements were performed on gender-balanced groups. Male mice were tested in a Morris water maze essentially as described (14); see *Supporting Text*, which is published as supporting information on the PNAS web site, www.pnas.org, for details. Anesthetized mice were flush-perfused transcardially with PBS. One hemibrain was fixed in 4% phosphate-buffered paraformaldehyde at 4°C for 48 h, and the other was stored at –70°C. All experiments were approved by the committee on animal research of the University of California, San Francisco.

Human Tissues. Fixed brain tissues of AD cases [nine women, six men; age 71–92 yr (83.7 ± 6.7, mean ± SD)] and nondemented controls (one woman, one man; age 71 and 74 yr) were from the Alzheimer's Disease Research Center (University of California at San Diego). AD was determined according to criteria of the Consortium to Establish a Registry for Alzheimer's Disease and the National Institute on Aging. Formalin-fixed hippocampal tissues were postfixed for 72 h in 4% phosphate-buffered paraformaldehyde.

Immunohistochemistry. Vibratome sections (50 μm, mouse; 40 μm, human) or sliding microtome sections (30 μm, mouse) were used for fluorescence double-labeling or staining with standard avidin–biotin/peroxidase methods. After quenching endogenous peroxidase activity and blocking nonspecific binding, sections were incubated first with rabbit anticalbindin (1:15,000, Swant, Bellinzona, Switzerland); rabbit anti-c-Fos (1:10,000, Ab-5, Oncogene); mouse mAb anti-Neu-N (1:5,000, Chemicon); or mouse mAb anti-Aβ (1:500, 3D6, Elan Pharmaceuticals, South San Francisco, CA), and then with fluorescein-labeled donkey anti-rabbit (1:300, Jackson ImmunoResearch); Texas red-labeled donkey anti-mouse (1:300, Jackson ImmunoResearch); biotinylated goat anti-rabbit (1:200, Vector Laboratories); or biotinylated goat anti-mouse (1:600, Vector Laboratories). Diaminobenzidine was used as a chromagen. Immunofluorescence was visualized by confocal microscopy.

Abbreviations: Aβ, amyloid-β peptides; AD, Alzheimer's disease; CB, calbindin-D_{28k}; hAPP, human amyloid precursor proteins; $hAPP_{FAD}$, familial AD-mutant hAPP; $hAPP_{WT}$, WT hAPP; IR, immunoreactivity/immunoreactive; TG, transgenic.

†Present address: Departments of Behavioral Neuroscience and Neurology, Oregon Health and Science University, Portland, OR 97239.

§To whom correspondence should be addressed. E-mail: lmucke@gladstone.ucsf.edu.

www.pnas.org/cgi/doi/10.1073/pnas.1133381100

Quantitation of Immunoreactive Structures. Digitized images were obtained with a DEI-470 digital camera (Optronics, Goleta, CA) on a BX-60 microscope (Olympus, Melville, NY). For calbindin-D_{28k} (CB) immunoreactivity (IR), two coronal sections (300 μm apart) per mouse between –2.54 and –2.80 mm from bregma were selected. Integrated optical density (IOD) was determined with BioQuant Image Analysis (R&M Biometrics, Nashville, TN) and averaged in two areas (0.04 mm^2 each) of the molecular layer of the dentate gyrus and of the stratum radiatum of the CA1 region. Relative CB-IR levels were expressed as the ratio of IODs in the molecular layer and in the stratum radiatum of the same section. The mean ratio of non-TGs was defined as 1.0. Relative numbers of c-Fos-IR granule cells were determined by counting c-Fos-IR cells in the granular layer in every 10th serial coronal section throughout the rostrocaudal extent of the granular layer. The average percentage area of the hippocampus occupied by Aβ-IR deposits was determined in four coronal sections (300 μm apart) per mouse.

Western Blot and Quantitative Fluorogenic RT-PCR. Hemibrains were sectioned with a vibratome into 450-μm sagittal slices, and the dentate gyrus was microdissected on ice. For protein analysis, dentate gyrus samples were individually sonicated at 4°C in buffer containing 10 mM Hepes at pH 7.4, 150 mM NaCl, 50 mM NaF, 1 mM EDTA, 1 mM DTT, 1 mM PMSF, 1 mM Na_3VO_4, 10 μg/ml leupeptin, 10 μg/ml aprotinin, and 1% SDS and centrifuged at 5,000 $\times$ *g* (10 min). Equal amounts of protein (by Bradford assay) were resolved by SDS/PAGE and transferred to nitrocellulose membranes. After blocking, membranes were labeled with rabbit anti-CB (1:20,000, Swant); mouse mAb anti-hAPP (1:1,000, 8E5, Elan Pharmaceuticals); or mouse mAb anti-α-tubulin (1:100,000, B512, Sigma), and incubated with horseradish peroxidase-conjugated goat anti-rabbit IgG (1:5,000, Chemicon) or goat anti-mouse IgG (1:10,000, Chemicon). Bands were visualized by enhanced chemiluminescence and quantitated by densitometry and QUANTITY ONE 4.0 software (Bio-Rad).

For quantitative fluorogenic RT-PCR, RT reactions contained 120 ng of total RNA (DNase-treated) and random hexamer plus oligo d(T) primers. Diluted reactions were analyzed with SYBR green PCR reagents and an ABI Prism 7700 sequence detector (Applied Biosystems). cDNA levels of CB, hAPP, and GAPDH were determined relative to standard curves from pooled samples. The slope of standard curves, control reactions without RT, and dissociation curves of products indicated adequate PCR quality. Primers: CB, 5′-GGAAAGGAGCTGCAGAACTTGAT-3′, 5′-TTCCGGTGATAGCTCCAATCC-3′; hAPP, 5′-GAGGAGGATGACTCGGATGTCT-3′, 5′-AGCCACTTCTTCCTCCTCTGCTA-3′; GAPDH, 5′-GGGAAGCCCATCACCATCTT-3′, 5′-GCCTTCTCCATGGTGGTGAA-3′.

Results

CB Levels Are Reduced in the Dentate Gyrus of $hAPP_{FAD}$ Mice and Humans with AD. CB is abundant in hippocampal neurons, particularly in granule cells of the dentate gyrus and pyramidal cells of the CA1 region (25). Neuronal CB levels were significantly reduced in $hAPP_{FAD}$ mice (Figs. 1*A* and 2*B*), primarily in the granular layer of the dentate gyrus and in the molecular layer into which the granule cells extend their dendrites. Pyramidal cells in CA1 and their dendrites in the stratum radiatum were unaffected (Figs. 1*A* and 2*B*). Double-labeling of brain sections from $hAPP_{FAD}$ mice for CB and the neuronal marker Neu-N (Fig. 1*B*) indicated that the CB reductions in the dentate gyrus primarily reflected a decrease in neuronal CB levels rather than loss of CB-producing neurons.

Although loss of CB-positive neurons in cortical areas of AD cases has been described (26, 27), we found no studies reporting CB reductions in granule cells of the dentate gyrus in AD. In fact, granule cells are relatively resistant to AD-associated cell death (28). Yet, we found marked reductions in neuronal CB-IR in the dentate gyrus of AD cases, with the most striking depletions seen in the most severely demented individuals (Fig. 1*D*).

CB Reductions Depend on Age, Aβ, and Reduced CB mRNA Levels. CB reduction in $hAPP_{FAD}$ mice was age-dependent (Fig. 2*A*). Significant CB reductions in $hAPP_{FAD}$ mice were also detected at 6–7, 9–11, and 14–15 mo [n = 4–8 mice per age and genotype (not shown)]. hAPP mice from line I5, which express $hAPP_{WT}$ and have much lower Aβ levels than $hAPP_{FAD}$ mice from line J20 (6), had no significant reductions in CB at 6–9 mo (Fig. 2 *B* and *C*) or at 11–13 and 13–15 mo (not shown; n = 8–12 $hAPP_{WT}$ mice and n = 5–11 non-TG controls per age group). Reductions in CB-IR in 6- to 7-mo-old $hAPP_{FAD}$ mice correlated tightly with CB protein and mRNA levels in the dentate gyrus of the opposite hemibrain (Fig. 2 *C* and *D*), indicating a mechanism affecting gene expression.

CB Reductions in $hAPP_{FAD}$ Mice Are Associated with a Decrease in c-Fos-IR Neurons in the Dentate Gyrus. The immediate early gene *c-fos* is also critically dependent on calcium (23). The number of c-Fos-IR neurons in the granular layer of the dentate gyrus was significantly reduced in $hAPP_{FAD}$ mice even at 4–5 mo of age and decreased further by 6–7 mo (Figs. 1*C* and 2 *E* and *F*). Although interindividual variations in CB and c-Fos were substantial (Figs. 1*A* and 3*A*), the reductions were tightly correlated in $hAPP_{FAD}$ mice (Fig. 3*A*), suggesting the underlying mechanisms are nonrandom and overlapping.

Reductions in CB and c-Fos Correlate with Relative Abundance of Aβ1–42 but Not with Plaque Load or Gender. At 6–7 mo of age, when CB and c-Fos reductions were prominent, male (n = 22) and female (n = 20) $hAPP_{FAD}$ mice showed no significant differences ($P > 0.25$) in the levels of CB-IR, c-Fos-IR granule cells, and percent area occupied by 3D6-IR Aβ deposits (data not shown). In the dentate gyrus of 6- to 7-mo-old $hAPP_{FAD}$ mice (n = 9), CB mRNA, protein, and IR did not correlate with levels of $hAPP_{FAD}$ mRNA or protein ($P > 0.7$ for all six CB–$hAPP_{FAD}$ correlations, not shown), suggesting that the CB reductions are not caused by the expression of $hAPP_{FAD}$ per se.

CB and c-Fos reductions in $hAPP_{FAD}$ mice also did not correlate with early Aβ deposition (Fig. 3*B*). When analyzed over a wider age range (4–22 mo), these reductions did not correlate with plaque load either ($P > 0.6$). However, they did correlate with Aβ1–42/Aβ1–x ratios (Fig. 3*C*), which reflect the abundance of Aβ ending at residue 42 relative to other, mostly shorter, Aβ peptides (29, 30).

Reductions in CB and c-Fos in the Dentate Gyrus of $hAPP_{FAD}$ Mice Correlate Tightly with Deficits in Learning and Memory. To further assess the pathophysiological significance of CB and c-Fos reductions in $hAPP_{FAD}$ mice, we analyzed mice in a Morris water maze test (14), which is widely used to assess learning and memory (31). Behavioral deficits in $hAPP_{FAD}$ mice showed a striking relationship to neuronal reductions of CB and c-Fos in the dentate gyrus (Fig. 4).

The majority of $hAPP_{FAD}$ mice learned to navigate to a visible platform, demonstrating efficient cued learning (sessions 1–4), but showed significant deficits in the spatial component of the test, during which they had to use extramaze cues to locate a hidden platform in the pool (sessions 5–10) (Fig. 4*A*). These $hAPP_{FAD}$ mice were also impaired in the probe trial (Fig. 4*B*), which provides a putative measure of memory retention. In contrast, they did not differ from non-TG controls in swim speed

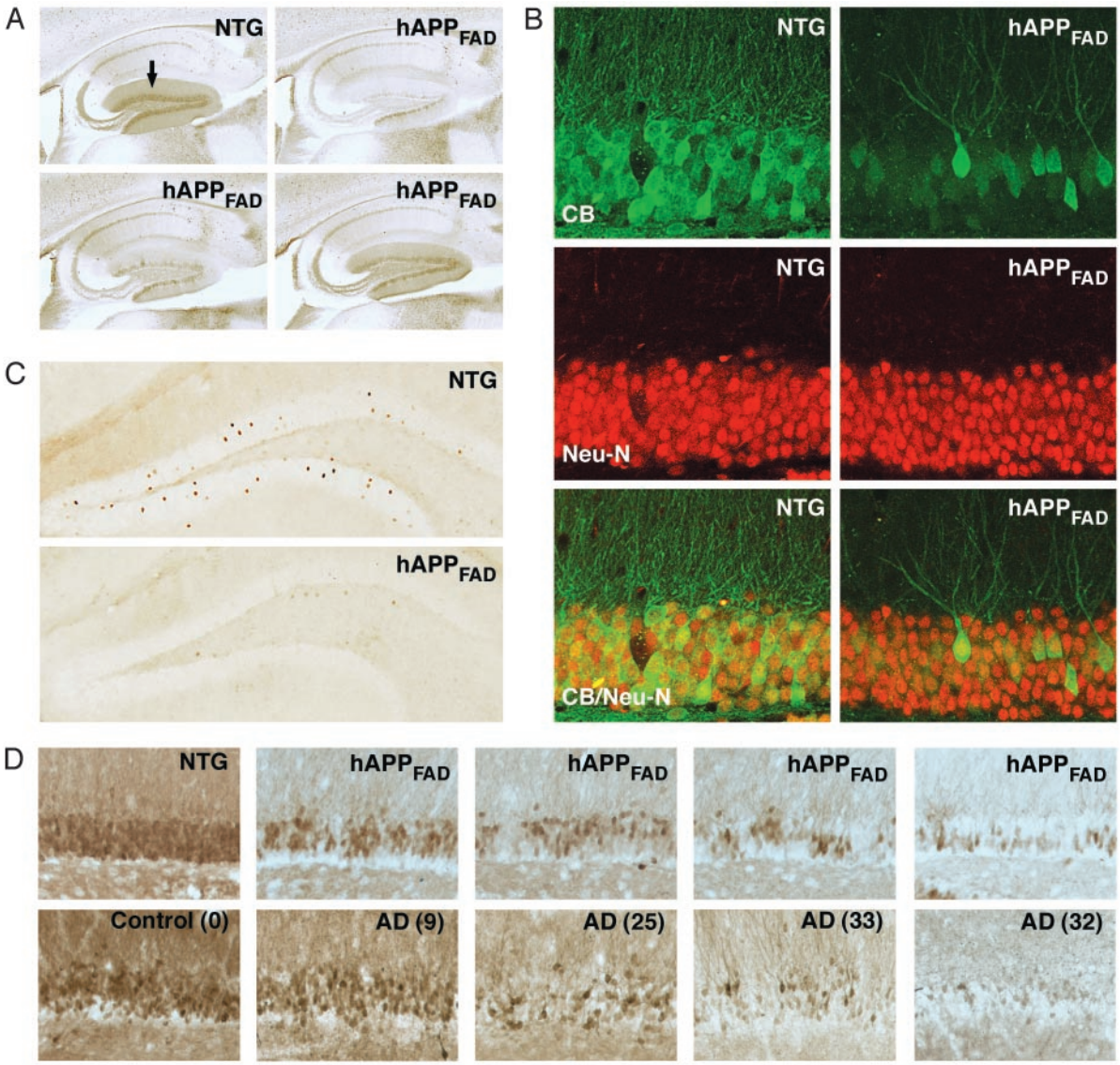

Fig. 1. CB and c-Fos reductions in the dentate gyrus of hAPP$_{FAD}$ mice and humans with AD. Brain sections from 6- to 7-mo-old mice were immunolabeled for CB, c-Fos, or the neuronal marker Neu-N. (*A*) Sagittal vibratome sections illustrating typical CB-IR in the dentate gyrus (arrow) of a non-TG mouse and a range of CB reductions in hAPP$_{FAD}$ mice. (*B*) Double-labeling of sagittal vibratome sections for CB (green) and Neu-N (red) did not reveal obvious changes in the density of neuronal nuclei in the CB-depleted granular layer of hAPP$_{FAD}$ mice. (*C*) Coronal sections illustrating the decrease in c-Fos-IR neurons in the granular layer of hAPP$_{FAD}$ mice. (*D*) Hippocampal sections from 6- to 7-mo-old hAPP$_{FAD}$ mice (*Upper*) and AD cases (*Lower*) were stained for CB. A comparable range of CB reductions was found in the granular layer of hAPP$_{FAD}$ mice and AD cases. Numbers in parentheses indicate Blessed score, which increases with the severity of the dementia.

(Fig. 4*C*), suggesting that their longer escape latencies during the hidden platform sessions were not due to motor deficits.

CB levels in the dentate gyrus did not correlate with cued learning in non-TG mice or in hAPP$_{FAD}$ mice with deficits in spatial, but not cued, learning (Fig. 4*D*). CB levels were also unrelated to performance in the first two sessions of the hidden platform training (Fig. 4*E*, sessions 5 and 6) before significant spatial learning was evident in non-TG mice (Fig. 4*A*). However, in hAPP$_{FAD}$ mice, CB levels correlated tightly with spatial learning deficits in the last four sessions of hidden platform training (Fig. 4*E*, sessions 7–10), when spatial learning was clearly evident in non-TG controls (Fig. 4*A*). This correlation remained strong when escape latencies or path lengths were averaged over all hidden platform trials (Fig. 4*F*). The relative level of c-Fos-IR granule cells also correlated well with spatial learning in hAPP$_{FAD}$ mice but not in non-TG controls (Fig. 4*G*).

Some hAPP$_{FAD}$ mice were excluded from the above analysis because they had significant deficits even in cued learning (Fig. 4*H*), which confounds the interpretation of deficits in the spatial component of this test (31). These mice had the most prominent reductions in both CB and c-Fos-IR granule cells (Fig. 4*I*).

Discussion

Our study demonstrates a cause–effect relationship between the expression of hAPP$_{FAD}$/Aβ and age-dependent reductions in CB and c-Fos in a neuronal population critically involved in learning and memory. Reductions in these calcium-dependent proteins in granule cells of the dentate gyrus correlated tightly with spatial learning deficits in hAPP$_{FAD}$ mice and depended on the relative abundance of Aβ1–42 but not on the amount of Aβ deposited in plaques.

These findings support the hypothesis that AD-related neuronal deficits are caused by small nonfibrous Aβ assemblies rather than

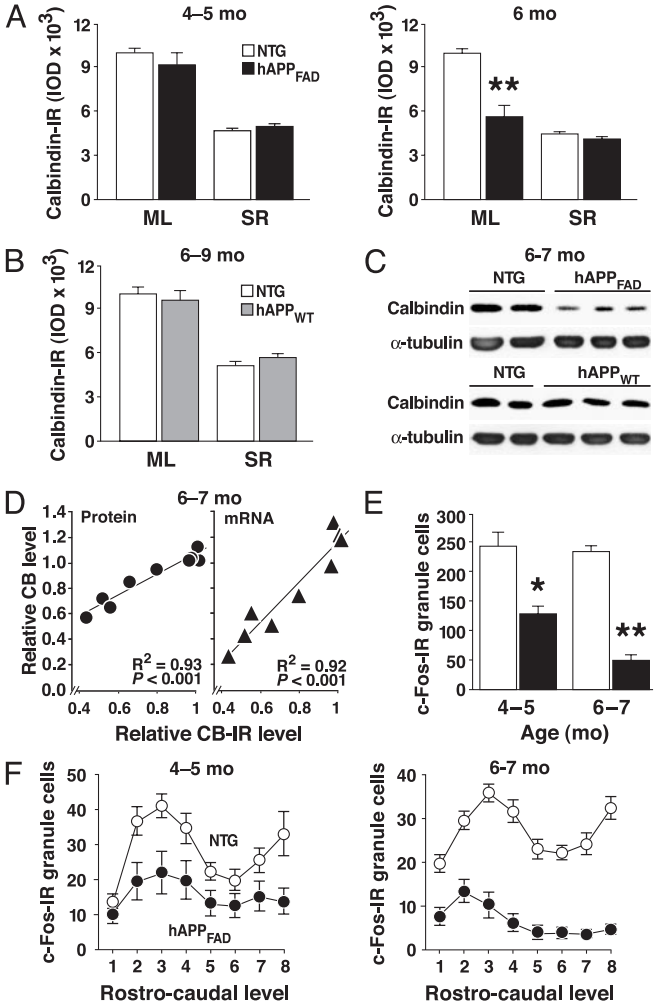

Fig. 2. CB and c-Fos reductions in the dentate gyrus depend on age and type of hAPP expressed. (*A* and *B*) Coronal brain sections were obtained from hAPP$_{FAD}$ mice, hAPP$_{WT}$ mice, and non-TG controls (NTG). Ages in months (mo) are indicated (*Top*) (n = 10–13 mice per age and genotype). IOD, integrated optical density; ML, molecular layer; SR, stratum radiatum. (*C* and *D*) Total protein and RNA were extracted from dentate gyrus samples. Levels of CB protein (*C* and *D Left*) and mRNA (*D Right*) were determined by Western blot analysis and quantitative fluorogenic RT-PCR, respectively. Values obtained in different hAPP$_{FAD}$ mice were expressed as CB/α-tubulin (*D Left*) and CB/GAPDH (*D Right*) ratios. (*E* and *F*) The relative number of c-Fos-IR neurons in the granular layer was determined in coronal sections from hAPP$_{FAD}$ mice (black columns and dots) and non-TG controls (empty columns and dots) (n = 13–18 mice per age and genotype). Data represent group means for all sections analyzed (*E*) or for different rostrocaudal levels of the dentate gyrus (*F*). *, $P < 0.05$; **, $P < 0.001$.

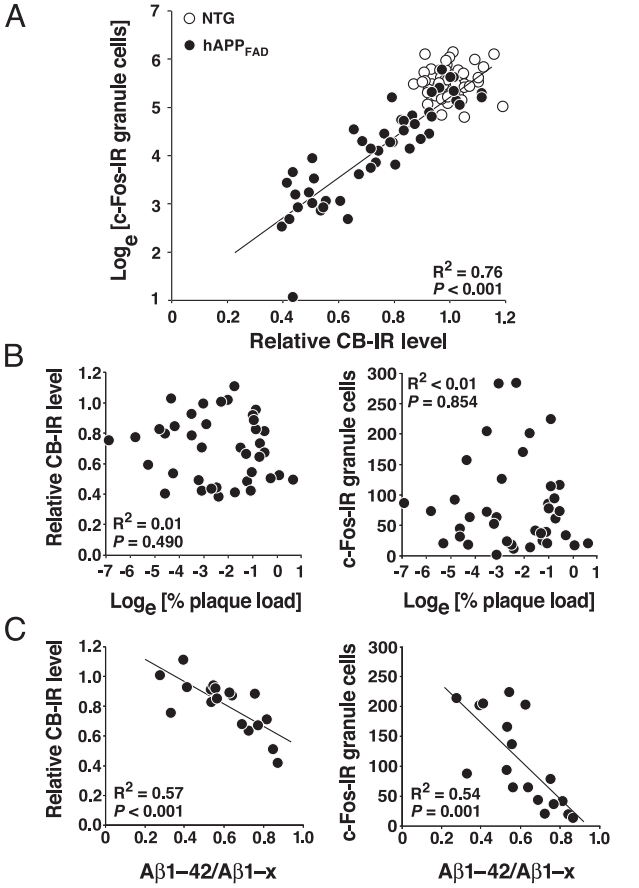

Fig. 3. Relationship among CB, c-Fos, plaque load, and Aβ levels. Brain sections and hippocampi were from hAPP$_{FAD}$ mice (black dots) and non-TG controls (empty dots). The square of correlation coefficients (R^2) and P values refer to hAPP$_{FAD}$ mice only. (*A*) Relative levels of CB and c-Fos-IR granule cells in the dentate gyrus were strongly correlated in hAPP$_{FAD}$ mice but not in non-TG controls (n = 48–60 per genotype; age, 4–7 mo). (*B*) Levels of CB and c-Fos-IR granule cells did not correlate with hippocampal plaque load in hAPP$_{FAD}$ mice with early plaque formation (n = 39; age, 4–7 mo). (*C*) Hippocampal levels of Aβ1–42 and Aβ1–x (approximates total Aβ) were determined by ELISA as described (6, 29) in hAPP$_{FAD}$ mice (n = 18 females) over a wider range of ages (4–22 months; mean ± SD, 10.7 ± 6.7 mo).

by plaques (4, 6, 8, 14, 15). Although Aβ production depends on hAPP levels, the formation of neurotoxic Aβ assemblies may be influenced by many other variables including the Aβ1–42/Aβ1–40 ratio and interindividual differences in the level or activity of proteins that bind or degrade Aβ (32–34). This may explain why reductions in CB and c-Fos in hAPP$_{FAD}$ mice correlated with the relative abundance of Aβ1–42 but not with hAPP$_{FAD}$ levels.

Although the exact mechanisms by which Aβ assemblies may reduce CB and c-Fos levels in granule cells remain to be determined, they might involve alterations in the function of calcium channels and other membrane proteins, chronic inflammation, and formation of pores in cell membranes, both in the dentate gyrus and in regions projecting to it (6, 21, 35–41).

The behavioral testing of mice is time consuming, and test results obtained in different laboratories can vary (42, 43). Plaque load is the most widely used pathological outcome measure in the preclinical assessment of anti-Aβ treatments (9–13), although it does not appear to correlate with behavioral deficits (8, 13, 44). Our study suggests that biochemical and radiological measures reflecting CB levels in the dentate gyrus could improve the assessment of AD treatments by providing a more reliable surrogate marker of Aβ-induced neuronal dysfunction.

Some hAPP$_{FAD}$ mice have impairments not only in the spatial but also in the cued component of the water maze test (8) (Fig. 4 *H* and *I*). The mechanisms underlying these impairments might differ from those causing more selective spatial learning deficits quantitatively, qualitatively, or both. The visible and hidden platform components of the water maze test can involve overlapping cognitive functions (7). Extensions of deficits from one component to the other might have been fostered here by the visibility of extramaze cues and the small size of the marker indicating the platform location during cued trials (see *Supporting Text*), which could promote engagement of spatial learning mechanisms. Furthermore, AD affects many brain regions besides the hippocampus, combining spatial learning deficits with other cognitive impairments. Widespread neuronal expression

NEUROSCIENCE

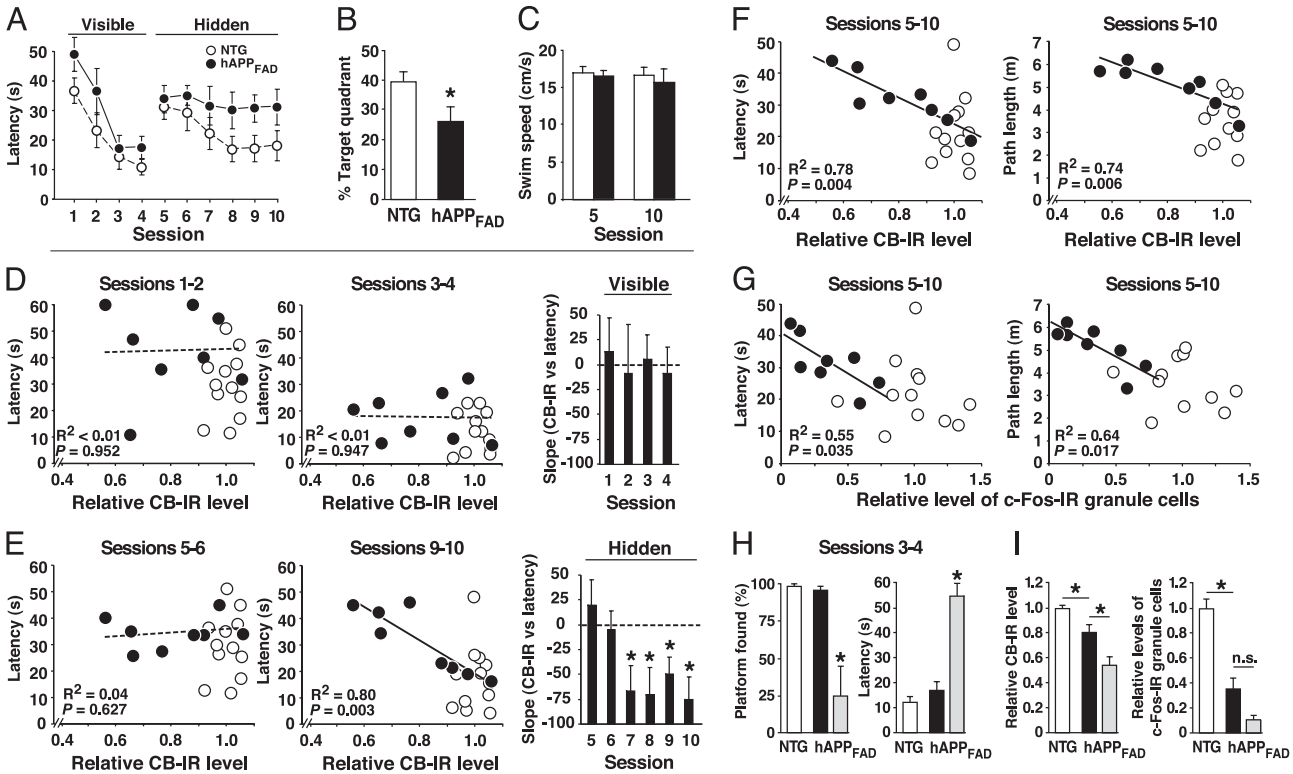

Fig. 4. Reductions in CB and c-Fos correlate tightly with behavioral deficits. hAPP$_{FAD}$ mice (black dots or columns) and non-TG littermate controls (empty dots and columns) (age 6–7 mo, all males) were trained in a Morris water maze. After behavioral testing, relative levels of CB and c-Fos-IR neurons in the dentate gyrus were measured. (*A–C*) Learning curves (*A*), probe trial performance (*B*), and average swim speeds (*C*) of non-TG controls ($n = 12$) and of hAPP$_{FAD}$ mice ($n = 8$) showing learning deficits when the platform was hidden but not when it was visible. Assessment of session effects in *A* by repeated-measures ANOVA revealed that hAPP$_{FAD}$ mice learned the cued task ($P < 0.001$) but not the spatial task ($P > 0.95$), whereas non-TG controls learned both tasks ($P < 0.001$). Average swim speeds in *C* were calculated for sessions 5 and 10 from all trials performed in the respective session. (*D* and *E*) Relationship of relative CB-IR levels and escape latencies during sessions in which the platform was visible (*D*) or hidden (*E*). See *A* for sequence of sessions. Filled and open circles represent mean latency values of individual mice calculated from the indicated sessions. Bars represent the slope coefficient ''*b*'' in the linear regression equation ($y = a + bx$) for hAPP$_{FAD}$ mice in the training sessions indicated. (*F*) Correlation of relative CB levels with average escape latencies (*Left*) and path lengths (*Right*) calculated from all sessions of hidden platform training. CB levels did not correlate with average swim speeds in the visible ($P = 0.86$) or hidden ($P = 0.47$) platform component of the test. (*G*) Correlation of relative levels of c-Fos-IR granule cells with average escape latencies (*Left*) and path lengths (*Right*) calculated as in *F*. The mean number of c-Fos-IR granule cells identified in non-TG controls was arbitrarily defined as 1.0. (*H*) Four hAPP$_{FAD}$ mice (gray columns) were excluded from the above analysis, because they showed a significant deficit in the visible platform training, defined here as an average latency (mean of all trials in sessions 3 and 4) exceeding the average latency plus two SD in non-TG controls. In contrast to the other mice, this group of hAPP$_{FAD}$ mice did not consistently find the visible platform. (*I*) Relative levels of CB and c-Fos-IR granule cells in non-TG contols and hAPP$_{FAD}$ mice that did or did not show deficits in the visible platform training. *, $P < 0.05$. R^2 and P values in (*D–G*) refer to hAPP$_{FAD}$ mice only; no significant correlations were identified in non-TG controls.

of hAPP$_{FAD}$/Aβ may have similar effects in severely impaired TG mice.

Our results demonstrate that neuronal populations resisting cell death in AD (28) can still be drastically altered at the molecular level. The marked reduction of CB in the dentate gyrus of patients with sporadic AD demonstrates that FAD mutations are not necessary for such reductions to occur in the human condition. Aβ42/Aβ40 ratios high enough to elicit CB reductions within 6 mo may be attainable in hAPP mice only by the introduction of FAD mutations, whereas Aβ42/Aβ40 ratios in sporadic AD may be high enough to deplete CB levels over time even in the absence of FAD mutations. More cases will need to be analyzed to establish the extent to which CB reductions correlate with cognitive deficits in AD.

Although it is likely that diverse molecular alterations contribute to AD-associated neuronal dysfunction, the tight association between molecular and functional alterations we identified raises the question of whether reductions in CB and c-Fos not only indicate but also mediate hAPP$_{FAD}$/Aβ-dependent behavioral deficits. Because CB can protect neurons against Aβ-induced toxicity (45), the reduction of CB by Aβ could be part of a vicious cycle promoting progressive neuronal dysfunction in hAPP$_{FAD}$ mice and in AD. Inhibiting CB expression impaired water maze learning in TG mice (46) and prolonged increases in intraneuronal calcium after stimulation of hippocampal slices (36). Ablation of CB also worsened neuronal deficits in a TG model of spinocerebellar ataxia-1 (47), another neurodegenerative disease with abnormal protein accumulation. Ablation or inhibition of c-Fos elicited deficits in the water maze test and related tasks (23, 48).

These findings suggest that reductions in CB and c-Fos in hAPP$_{FAD}$ mice and humans with AD may not only reflect cognitive deficits but may contribute to them. The roles of these and related molecular alterations as potential indicators and mediators of neurodegenerative disease merit further investigation.

We thank Hilda Ordanza, Kristina Shockley, and Anthony LeFevour for excellent technical support; Christian Essrich for contributing RT-PCR data; Gary Howard and Stephen Ordway for editorial review; and Denise McPherson for administrative assistance. This work was supported by National Institutes of Health Grants AG11385, NS43945, and NS41787 (to L.M.) and by fellowships from the Spanish Ministry of Education, Culture, and Sport (to J.J.P.) and the John Douglas French Alzheimer's Foundation (to J.C.).

1. Cowan, W. M. & Kandel, E. R. (2001) *J. Am. Med. Assoc.* **285,** 594–600.
2. Games, D., Adams, D., Alessandrini, R., Barbour, R., Berthelette, P., Blackwell, C., Carr, T., Clemens, J., Donaldson, T., Gillespie, F., *et al.* (1995) *Nature* **373,** 523–527.
3. Dodart, J. C., Meziane, H., Mathis, C., Bales, K. R., Paul, S. M. & Ungerer, A. (1999) *Behav. Neurosci.* **113,** 982–990.
4. Hsia, A., Masliah, E., McConlogue, L., Yu, G., Tatsuno, G., Hu, K., Kholodenko, D., Malenka, R. C., Nicoll, R. A. & Mucke, L. (1999) *Proc. Natl. Acad. Sci. USA* **96,** 3228–3233.
5. Moechars, D., Dewachter, I., Lorent, K., Reverse, D., Baekelandt, V., Naidu, A., Tesseur, I., Spittaels, K., Van Den Haute, C., Checler, F., *et al.* (1999) *J. Biol. Chem.* **274,** 6483–6492.
6. Mucke, L., Masliah, E., Yu, G.-Q., Mallory, M., Rockenstein, E. M., Tatsuno, G., Hu, K., Kholodenko, D., Johnson-Wood, K. & McConlogue, L. (2000) *J. Neurosci.* **20,** 4050–4058.
7. Arendash, G. W. & King, D. L. (2002) *Physiol. Behav.* **75,** 643–652.
8. Westerman, M. A., Cooper-Blacketer, D., Mariash, A., Kotilinek, L., Kawarabayashi, T., Younkin, L. H., Carlson, G. A., Younkin, S. G. & Ashe, K. H. (2002) *J. Neurosci.* **22,** 1858–1867.
9. Cherny, R. A., Atwood, C. S., Xilinas, M. E., Gray, D. N., Jones, W. D., McLean, C. A., Barnham, K. J., Volitakis, I., Fraser, F. W., Kim, Y. S., *et al.* (2001) *Neuron* **30,** 665–676.
10. Lim, G. P., Yang, F., Chu, T., Gahtan, E., Ubeda, O., Beech, W., Overmier, J. B., Hsiao-Ashe, K., Frautschy, S. A. & Cole, G. M. (2001) *Neurobiol. Aging* **22,** 983–991.
11. McLaurin, J., Cecal, R., Kierstead, M. E., Tian, X., Phinney, A. L., Manea, M., French, J. E., Lambermon, M. H. L., Darabie, A. A., Brown, M. E., *et al.* (2002) *Nat. Med.* **8,** 1263–1269.
12. Schenk, D. (2002) *Nature* **3,** 824–828.
13. Dodart, J. C., Bales, K. R., Gannon, K. S., Greene, S. J., DeMattos, R. B., Mathis, C., DeLong, C. A., Wu, S., Wu, X., Holtzman, D. M., *et al.* (2002) *Nat. Neurosci.* **5,** 452–457.
14. Raber, J., Wong, D., Yu, G.-Q., Buttini, M., Mahley, R. W., Pitas, R. E. & Mucke, L. (2000) *Nature* **404,** 352–354.
15. Klein, W. L., Krafft, G. A. & Finch, C. E. (2001) *Trends Neurosci.* **24,** 219–224.
16. Buttini, M., Yu, G.-Q., Shockley, K., Huang, Y., Jones, B., Masliah, E., Mallory, M., Yeo, T., Longo, F. M. & Mucke, L. (2002) *J. Neurosci.* **22,** 10539–10548.
17. Braak, H. & Braak, E. (1998) *J. Neural Transm.* **105,** Suppl. 53, 127–140.
18. Thal, D. R., Rüb, U., Orantes, M. & Braak, H. (2002) *Neurology* **58,** 1791–1800.
19. Burgess, N., Maguire, E. A. & O'Keefe, J. (2002) *Neuron* **35,** 625–641.
20. Berridge, M. J. (1998) *Neuron* **21,** 13–26.
21. Mattson, M. P. & Chan, S. L. (2001) *J. Mol. Neurosci.* **17,** 205–224.
22. Carafoli, E. (2002) *Proc. Natl. Acad. Sci. USA* **99,** 1115–1122.
23. Guzowski, J. F. (2002) *Hippocampus* **12,** 86–104.
24. Rockenstein, E. M., McConlogue, L., Tan, H., Gordon, M., Power, M., Masliah, E. & Mucke, L. (1995) *J. Biol. Chem.* **270,** 28257–28267.
25. Celio, M. R. (1990) *Neuroscience* **35,** 375–475.
26. Ichimiya, Y., Emson, P. C., Mountjoy, C. Q., Lawson, D. E. M. & Heizmann, C. W. (1988) *Brain Res.* **475,** 156–159.
27. Hof, P. R. & Morrison, J. H. (1991) *Exp. Neurol.* **111,** 293–301.
28. West, M. J., Coleman, P. D., Flood, D. G. & Troncoso, J. C. (1994) *Lancet* **344,** 769–772.
29. Johnson-Wood, K., Lee, M., Motter, R., Hu, K., Gordon, G., Barbour, R., Khan, K., Gordon, M., Tan, H., Games, D., *et al.* (1997) *Proc. Natl. Acad. Sci. USA* **94,** 1550–1555.
30. Gouras, G. K., Xu, H., Jovanovic, J. N., Buxbaum, J. D., Wang, R., Greengard, P., Relkin, N. R. & Gandy, S. (1998) *J. Neurochem.* **71,** 1920–1925.
31. D'Hooge, R. & De Deyn, P. P. (2001) *Brain Res. Rev.* **36,** 60–90.
32. Lambert, M. P., Barlow, A. K., Chromy, B. A., Edwards, C., Freed, R., Liosatos, M., Morgan, T. E., Rozovsky, I., Trommer, B., Viola, K. L., *et al.* (1998) *Proc. Natl. Acad. Sci. USA* **95,** 6448–6453.
33. Selkoe, D. J. (2001) *Neuron* **32,** 177–180.
34. Stine, W. B., Jr., Dahlgren, K. N., Krafft, G. A. & LaDu, M. J. (2003) *J. Biol. Chem.* **278,** 11612–11622.
35. Heyser, C. J., Masliah, E., Samimi, A., Campbell, I. L. & Gold, L. H. (1997) *Proc. Natl. Acad. Sci. USA* **94,** 1500–1505.
36. Pasti, L., Carmignoto, G., Pozzan, T., Battini, R., Ferrari, S., Lally, G. & Emson, P. C. (1999) *NeuroReport* **10,** 2367–2372.
37. Nägerl, U. V., Mody, I., Jeub, M., Lie, A. A., Elger, C. E. & Beck, H. (2000) *J. Neurosci.* **20,** 1831–1836.
38. Dineley, K. T., Westerman, M., Bui, D., Bell, K., Ashe, K. H. & Sweatt, J. D. (2001) *J. Neurosci.* **21,** 4125–4133.
39. Lin, H., Bhatia, R. & Lal, R. (2001) *FASEB J.* **15,** 2433–2444.
40. Wyss-Coray, T. & Mucke, L. (2002) *Neuron* **35,** 419–432.
41. Redwine, J. M., Kosofsky, B., Jacobs, R. E., Games, D., Reilly, J. F., Morrison, J. H., Young, W. G. & Bloom, F. E. (2003) *Proc. Natl. Acad. Sci. USA* **100,** 1381–1386.
42. Crabbe, J. C., Wahlsten, D. & Dudek, B. C. (1999) *Science* **284,** 1670–1672.
43. Wahlsten, D., Metten, P., Phillips, T. J., Boehm, S. L., II, Burkhart-Kasch, S., Dorow, J., Doerksen, S., Downing, C., Fogarty, J., Rodd-Henricks, K., *et al.* (2003) *J. Neurobiol.* **54,** 283–311.
44. Holcomb, L. A., Gordon, M. N., Jantzen, P., Hsiao, K., Duff, K. & Morgan, D. (1999) *Behav. Genet.* **29,** 177–185.
45. Guo, Q., Christakos, S., Robinson, N. & Mattson, M. P. (1998) *Proc. Natl. Acad. Sci. USA* **95,** 3227–3232.
46. Molinari, S., Battini, R., Ferrari, S., Pozzi, L., Killcross, A. S., Robbins, T. W., Jouvenceau, A., Billard, J.-M., Dutar, P., Lamour, Y., *et al.* (1996) *Proc. Natl. Acad. Sci. USA* **93,** 8028–8033.
47. Vig, P. J. S., Subramony, S. H. & McDaniel, D. O. (2001) *Brain Res. Bull.* **56,** 221–225.
48. He, J., Yamada, K. & Nabeshima, T. (2002) *Neuropsychopharmacology* **26,** 259–268.